Cyclic loading response and associated yield criteria for soft railway subgrade - Theoretical and experimental perspectives

Buddhima Indraratna[1]

Distinguished Professor of Civil Engineering,

Director, Transport Research Centre, University of Technology Sydney, Australia

Thanh Trung Nguyen

Research Fellow,

Transport Research Centre, University of Technology Sydney, Australia

Mandeep Singh

Senior Technical Support Officer (Geotech)
School of Civil and Environmental Engineering
University of Technology Sydney

Cholachat Rujikiatkamjorn

Professor of Civil Engineering,

Transport Research Centre, University of Technology Sydney, Australia

John P Carter

Emeritus Professor,

Faculty of Engineering and Built Environment,

University of Newcastle, Callaghan, NSW 2308, Australia

Ni Jing

Senior Lecturer

University of Shanghai for Science and Technology,

Shanghai, China

Minh Hoang Truong

PhD Candidate,

University of Wollongong, NSW 2522, Australia

Words: 6300; Figures: 11

Submitted to: Computers and Geotechnics

(Special Issue Commemorating Late Prof Scott Sloan)

[1]Corresponding author: Buddhima Indraratna (Buddhima.Indraratna@uts.edu.au

Abstract: Heavy haul rail transport certainly demands a more robust and stable railway foundation as the subgrade soils are prone to instability at higher axle loads. The current paper presents a series of cyclic triaxial tests to investigate the response of different subgrade soils with varying cyclic stress ratio (CSR). Theoretical models based on the Modified Cam Clay (MCC) model are extended to predict the experimental results. Two different hypotheses are proposed and discussed in this paper, namely, Model A: yield surface changes its size, and Model B: yield surface changes its shape, during cyclic loading. The results indicate that when CSR exceeds a critical threshold (CSR_c), the excess pore water pressure (EPWP) and axial strain (ε_{ac}) increase rapidly as the number of cycles (N) reaches a certain critical level ($N_{c,i}$). This causes soil instability and leads to specimen failure. At the same level of CSR, the faster the cyclic load is applied (i.e., at higher frequencies), the greater is the number of cycles required to trigger soil instability. The proposed models predict the inception of soil instability under cyclic rail loading with reasonable accuracy for Australian heavy haul track conditions.

Keywords: Heavy haul rail load, subgrade instability, cyclic stress ratio, excess pore water pressure, frequency

INTRODUCTION

The response of subgrade soil under repeated loads induced by the passage of trains has received increasing attention especially in recent decades. It may be attributed to the rising role of rail transport infrastructure which has put greater demand on having more stable and resilient track foundations. The demand for higher axle loads and train speeds has resulted in more frequent track failure and instability, such as subgrade fluidization and mud pumping (Trinh et al. 2012; Duong et al. 2014; Indraratna et al. 2020b; Nguyen and Indraratna 2021). Subgrade soils with low plasticity, when subjected to a high level of cyclic stress ratio (CSR), can fluidize under a rapid increase in excess pore water pressure (EPWP) and then pump upwards into the overlying materials including the topmost ballast layer (this is commonly known as mud pumping). For example, Fig. 1 shows track fouling induced by subgrade failure observed during many site investigations carried out by the authors in recent years. This results in severe degradation in the shear strength of the ballast and an overall excessive deformation of the track foundation, leading to substantial annual maintenance costs (Nguyen et al. 2019; Sydney Trains 2019). Therefore, significant efforts are needed to predict the response of subgrade soil under cyclic loading.

The cyclic loads induced by heavy-haul trains have a number of distinctive characteristics from other conventional cyclic loading sources (i.e., light transports and seismic excitations). Heavy-haul trains used for the mining industry can have an axle loads exceeding 35 tonnes, resulting in a high level of deviator stress (q) acting on the subgrade soil (Indraratna et al. 2010; Liu and Xiao 2010; Priest et al. 2010). Furthermore, the subgrade soil beneath rail tracks is usually subjected to low

confining pressures σ_c (typically around 15-40 kPa) resulting in a large magnitude of cyclic stress ratio (CSR), which is conventionally defined by the ratio between q and twice σ_c. It is also important to note that both the load and frequency magnitudes attenuate with depth of track substructure. Specifically, for heavy freight trains which normally travel with an average speed from 50 to 80 km/h, the frequency reduces significantly with depth over the ballast, capping and sub-ballast layers, resulting in loading frequency in a range from 1.0 to 5.0 Hz at 0.5-2 m depths of subgrade (Priest et al. 2010; Indraratna et al. 2011; Trinh et al. 2012; Mamou et al. 2017).

Fig. 1 Subgrade instability and associated contamination of overlying ballast along coastal railways in NSW, Australia

Several laboratory investigations have been conducted over the years to understand the cyclic behaviour of soils. While the majority of previous cyclic tests focussed on testing under high confining pressures and low frequency (i.e., < 1Hz) (Hyodo et al. 1994; Sakai et al. 2003; Baki et al. 2012), some recent studies investigated the cyclic behaviour of shallow soils under traffic loads (Trinh et al.

2012; Duong et al. 2014; Chawla and Shahu 2016). There has been a general lack of validation and calibration between experimental investigations and the constitutive response of subgrade soils under cyclic loads considering soil properties, the effect of CSR and loading frequency.

Modelling the constitutive behaviour of soil under cyclic loading has gained significant attention in the past years, resulting in various approaches ranging from simplified empirical equations to complex theories. One of the most prominent approaches which have received considerable attention in the past years is the use of multiple yield surfaces to model elastoplastic behaviour of soils under cyclic loading (Mróz et al. 1981; Zienkiewicz and Mróz 1984; Pastor et al. 1990; Li and Meissner 2002; Hong et al. 2014; Zhao et al. 2021). In this approach, complex rules and procedures associated with a large number of model parameters are required. For example, Li et al. (2011) estimate that these models need at least 12 different soil parameters in which majority are determined based on a series of experimental tests and analyses while some are based on past experience of model application. In contrast, empirical methods where accumulated EPWP and strain can be computed directly from soil and loading parameters such as the number of cycles and cyclic stress threshold based on some empirical multipliers are frequently used (Li and Selig 1996; Konstadinou and Georgiannou 2014; Nguyen et al. 2021). Despite simplicity in application, this approach cannot link coherently the predicted results to soil properties due to a lack of systematic theoretical background, leading to a wide variation of the model parameters.

Of the most well-balanced combination between simplicity and fundamental theoretical background, the use of the Modified Cam Clay (MCC) concept (Roscoe and Burland 1968) with consideration of yield surface evolution under cyclic load is

commonly preferred. For example, Carter et al. (1982) and later a study by Ni et al. (2015) assumed that the yield surface shrinks after each loading cycle, thus enabling the accumulated EPWP and plastic strain to be captured. In this approach, additional parameters are introduced to the MCC model to characterize the undrained cyclic behaviour. Although this model was applied successfully for soft cohesive soils (Ni et al. 2015), its major shortcoming lies in the prediction of volume change as the yield surface begins to shrink during unloading, contrary to the zero volume change constraint under undrained conditions.

In this current paper, a series of cyclic triaxial tests was carried out on different soils wherein, the loading condition aims to simulate the stress state of subgrade under rail tracks. The experimental results were used to validate recently proposed cyclic models which have been formulated based on the evolution of the yield surface due to cyclic loading.

EXPERIMENTAL INVESTIGATION

Methodology

A series of cyclic triaxial tests was performed on the reconstituted soils collected from vulnerable track sites along the South Coast rail line, NSW, Australia. Specifically, a subgrade soil sample (test Series II) was collected from a site showing signs of mud pumping and its response under cyclic loading was compared with Kaolin clay soil used in test Series I. All these soils had low to high (lower bound) plasticity index (PI), i.e., from 11 to 22 (see Table 1). The soils classify as highly compressible clay, CH (Series I) and low compressibility clay, CL (Series II). The critical stress ratios M of these soils were determined from static triaxial tests as shown in previous studies (Ni et al. 2015; Indraratna et al. 2020b). Note that these

values are relatively large for certain soils, however, they are still within the range of silty clay soils that have been reported elsewhere (Jefferies and Been 2015; Ouyang and Mayne 2018). The specimens were subjected to low confining stresses ($\sigma_3^{'}$ = 15-25 kPa, see Table 1) to simulate the shallow nature of the subgrade which is susceptible to instability. Given that the in situ subgrade stresses are anisotropic in nature, a ratio of horizontal to vertical stress of 0.6 was applied, based on a previous study (Nguyen and Indraratna 2019).

Test series	Soil description	Plasticity Index (*PI*)	*M*	Initial void ratio (e_o)	Confining pressure (kPa)	Load parameters		Reference
						CSR	f (Hz)	
I	Kaolin clay (CH)	22	1.68	1.32	25	0.1-0.3	1, 2 and 5	(Ni et al. 2015)
II	Silty clay (CL)	11	1.89	0.47	15	0.3-0.5	1	(Indraratna et al. 2020b)

Table 1 Properties of soil and loading used for laboratory investigations

Field data collected from subgrade beneath the rail tracks indicate that the stresses are essentially compressive in nature meaning the top of the subgrade experiences one-way cyclic stresses (Indraratna et al. 2010; Liu and Xiao 2010). Previous studies (Powrie et al. 2007; Indraratna et al. 2010; Trinh et al. 2012) show that the loading frequency acting on subgrade soil under ballasted track normally varies from 1 to 5 Hz considering a heavy haul train speed of less than 120 km/h. Therefore, a one-way stress-controlled loading scheme (ASTM D5311-92 2004) was adopted to simulate the cyclic stresses with frequency from 1- 5 Hz induced by the passage of the train. The cyclic response of the subgrade samples was studied using the cyclic triaxial apparatus which was setup on an axially stiff loading frame with an electromechanical actuator.

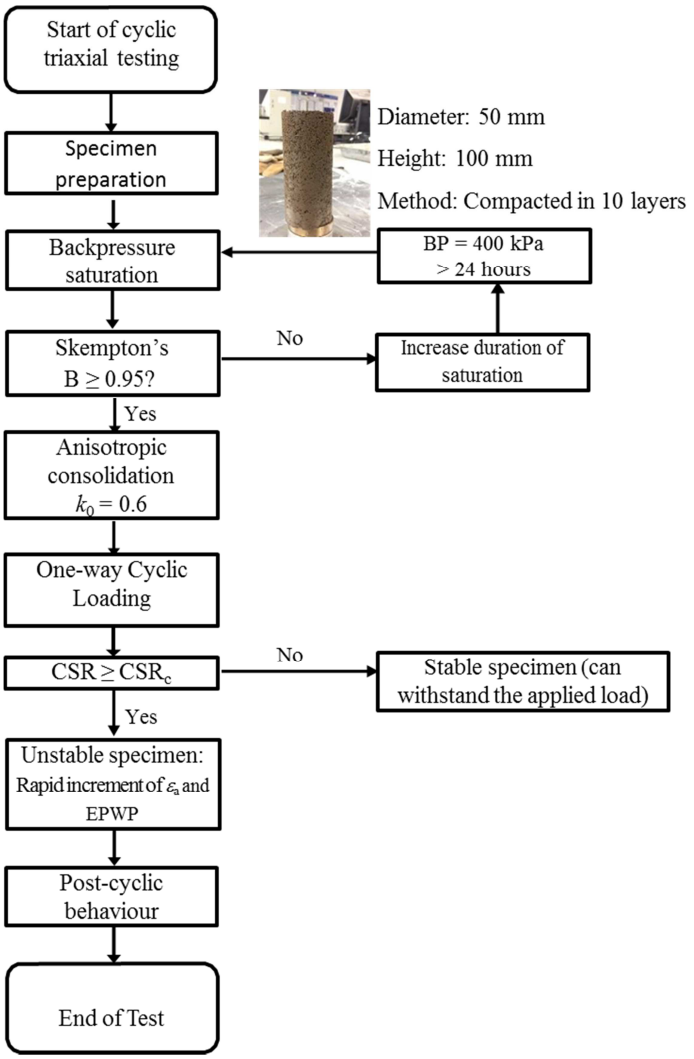

Fig. 2 Cyclic test procedure to investigate subgrade response to rail loading

CSR is defined as the ratio of the applied cyclic stress (σ_d) to twice the effective confining pressure ($\sigma_c^{'}$), as follows:

$$CSR = \frac{\sigma_d}{2\sigma_c^{'}} \quad (1)$$

In this study, CSR varying from 0.1 to 0.5 were considered. Note that while the CSR in the field can be larger than this range, the current study focuses on soft and relatively loose soils where CSR ≤ 0.5 are sufficient to cause instability. Fig. 2 shows

the flowchart adopted for the cyclic triaxial testing of soils to evaluate subgrade instability. Standard specimens (i.e., 50 mm diameter and 100 mm height) which were reconstituted from the initial raw soils were used in all tests. The soil specimens were subjected to an anisotropic consolidation process before the cyclic loading was applied. Cyclic load was applied only after the saturation degree of each specimen was satisfied, i.e., B > 0.95.

In the current study, the tests were terminated when either an axial strain of 10% was achieved or the number of loading cycles (N) reached 50,000. Note that this testing condition was set according to the worst scenario, albeit indeed there is a rest period between trains. Many heavy haul trains in Australia are 3-5 km long and they travel long distances (e.g. up to 300-400 km from mining source to the nearest port) at relatively low speeds of 60-80 km/h, which can induce about 600-1000 loading cycles per train. In extremely busy common freight networks used by different mining companies and other freight (e.g. agriculture produce), sometimes very long heavy haul trains do travel with relatively short time gaps between them. In order to capture the worst possible effects of EPWP build-up, the current study used 50,000 cycles continually without any rest period to observe the subgrade response.

Results and key findings

The experimental investigation of different soils indicated that when the CSR exceeds a certain critical threshold (CSR_c), the soil specimen experiences a rapid increase in EPWP and axial strain (ε_a) resulting in an unstable state of the soil. This is defined as soil instability. For example, Fig. 3 shows the response of EPWP and ε_a of the soil when CSR increases from 0.3 to 0.5. It is obvious that when CSR reaches 0.5, EPWP and ε_a begin to increase rapidly. Specifically, for CSR = 0.5,

EPWP and ε_a increase steeply when the number of cycles (*N*) exceeds a certain level, i.e., 30 which is considered as the critical number of cycles ($N_{c,i}$) required to cause soil instability. Any value of CSR < 0.5 results in a certain increase in EPWP and ε_a during the initial cycling but they become stable towards the end of the test (i.e., up to 50,000 cycles). Similar instability was observed from the results for Series I, albeit, at different critical levels of CSR and *N*, and this is due to the difference in soil properties.

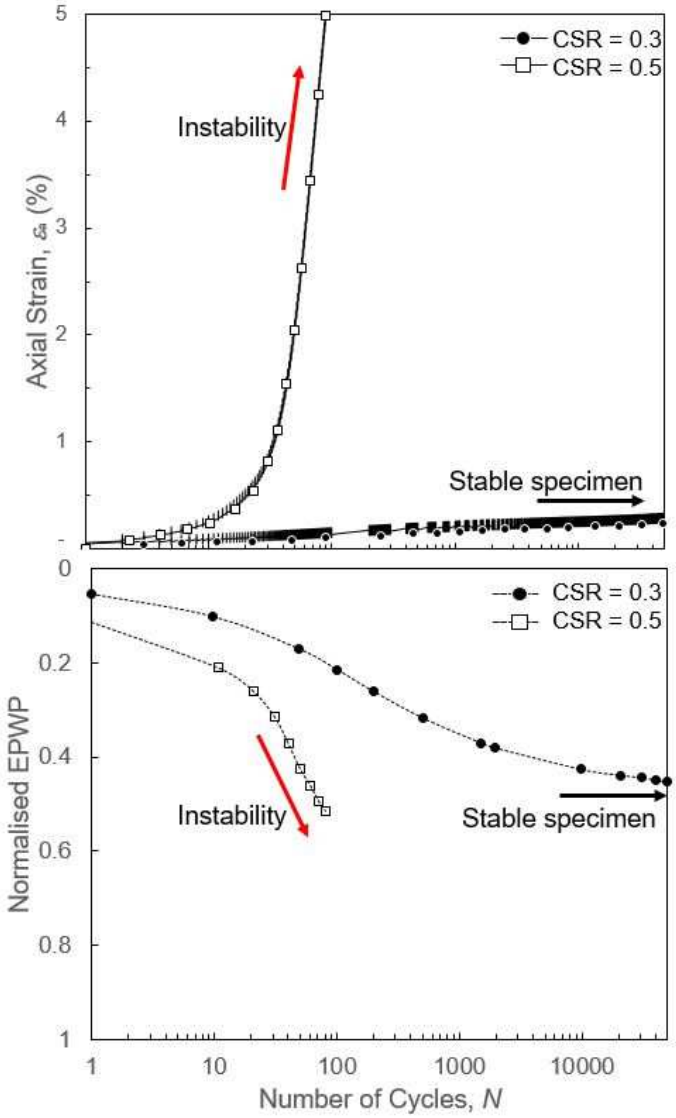

Fig. 3 Axial strain and normalised excess pore water pressure (EPWP) of soil (Series II) under increasing CSR (f = 1Hz, σ_c' = 25 kPa)

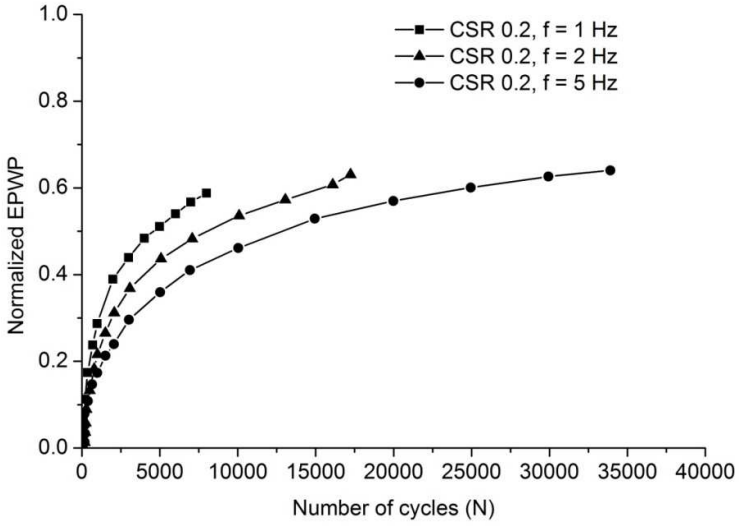

a)

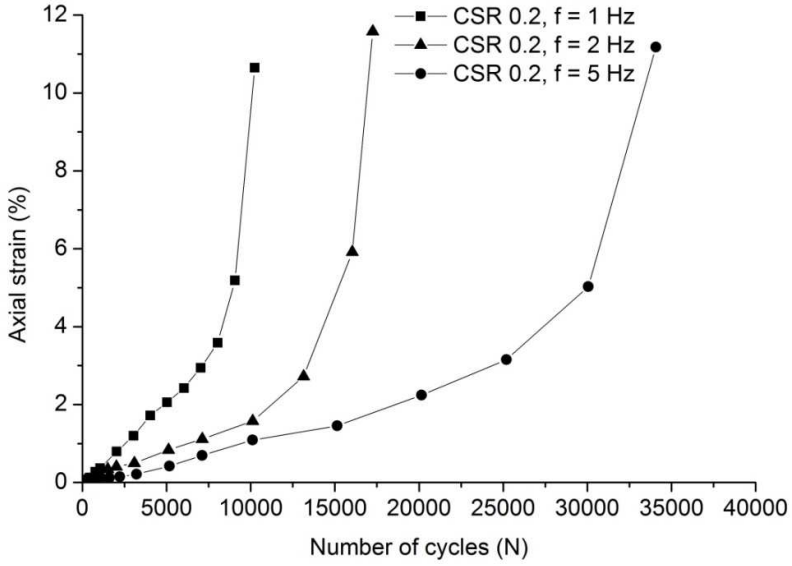

b)

Fig. 4 Variation in EPWP and axial strain of soil subjected to different loading frequencies (CSR = 0.2, σ_c' = 25 kPa, Series I).

Fig. 4 shows how different loading frequencies affect the response of soil under cyclic load (CSR = 0.2, Series I). The results show that the higher the frequency, the larger the number of cycles needed to cause soil instability. For example, for *f* = 1Hz, the axial strain of the soil sample begins to increase rapidly

when N exceeds around 7,500 cycles, whereas it takes more than 30,000 cycles to trigger instability of the soil for *f* = 5Hz. It is also noted that the soil becomes unstable with rapid development in axial strain when the normalized EPWP exceeds 0.6 despite varying loading frequency. In this analysis, the normalized EPWP is defined as the ratio between mean excess pore water pressure to the initial mean effective stress (p_o').

THEORETICAL CONCEPTS AND DEVELOPMENT

Theoretical background

As the models adopted in the current study are based on the framework of the modified Cam-Clay (MCC) theory, it is important to establish their fundamental elements, which are briefly summarized as follows for the convenient perusal of the readers. The mean effective stress p' and deviator stress q are computed by (Wood 1990):

$$p' = \left(\sigma_1' + 2\sigma_3'\right)/3 \tag{2}$$

$$q = \sigma_1 - \sigma_3 \tag{3}$$

$$\eta = q / p' \tag{4}$$

where σ_1' and σ_3' are the effective major and minor principal stress, respectively, whereas η is the stress ratio. The corresponding strain components are the volumetric strain ε_p and shear strain ε_q which are then calculated by (Wood 1990):

$$\varepsilon_p = \varepsilon_1 + 2\varepsilon_3 \tag{5}$$

$$\varepsilon_q = 2\left(\varepsilon_1 - \varepsilon_3\right)/3 \tag{6}$$

where ε_1 and ε_3 are the major and minor principal strains, respectively. The subscript *p* and *q* represent the volumetric and shear components, respectively. The incremental strains can be divided into elastic and plastic components as follows.

$$d\varepsilon_p = d\varepsilon_p^e + d\varepsilon_p^p \tag{7}$$

$$d\varepsilon_q = d\varepsilon_q^e + d\varepsilon_q^p \tag{8}$$

Elastic deformation

The volumetric and shear components of elastic strain increment develop as a result of change in p' and q, which is represented as follows (Wood 1990):

$$d\varepsilon_p^e = \kappa \frac{dp'}{vp'} \tag{9}$$

$$d\varepsilon_q^e = \frac{dq}{3G} \tag{10}$$

where v is the specific volume, κ is the gradient of unloading – reloading paths in the triaxial compression test, and *G* is the shear modulus.

Yield surface

The MCC yield surface is described in the $p' - q$ plane as follows (Wood 1990):

$$q^2 = M^2 p'^2 \left(\frac{p_0'}{p'} - 1 \right) \tag{11}$$

where p_o' is the hardening parameter and *M* is the stress ratio at critical state. Under static loading, the yield surface is an elliptical shape where its size is governed by two parameters p_o' and *M*.

Flow rule and plastic potential

In the MCC model, the associated flow rule is used, which means the plastic potential is the same as the yield surface (i.e., Eq. (11)).

Hardening rule

The conventional MCC defines the yield to expand (i.e., increase in p_o') when there is change in plastic volumetric strain, which can be represented by (Wood 1990):

$$\frac{dp_0^{'}}{d\varepsilon_p^p} = \frac{vp_0^{'}}{\lambda - \kappa} \tag{12}$$

and

$$\frac{dp_0^{'}}{d\varepsilon_q^p} = 0 \tag{13}$$

where λ is the gradient of the primary loading line in the triaxial compression plane, κ is the gradient of unloading – reloading paths in the triaxial compression test.

Yield surface response to cyclic loading

This section represents two different hypotheses where the behaviour of the yield surface is modified from the conventional MCC to simulate the response of soil under cyclic loading. In the first approach, the yield surface is assumed to change its size while retaining its shape during each unloading path, whereas the second approach assumes that the yield surface changes its shape but not the size, i.e., p_o' remains constant during unloading. Unloading is generally defined here as an initial reduction in the magnitude of the deviator stress. The first approach is inspired by the original work of Carter (1982), and subsequently extended with success in later studies (Gens and Potts 1988; Ni et al. 2015; Tachibana et al. 2020), while the

second approach, introduced for the first time in this paper, is based on the change in the shape of the yield surface. The governing equations and the processes involved in these 2 approaches, i.e., Models A and B, are given in detail as follows.

Model A: The size of yield surface shrinks during unloading (shape remains the same)

The rate that the yield surface shrinks its size over the number of cycles (*N*) can be governed by:

$$\frac{dp_0^{'}}{p_0^{'}} = \theta^* \frac{dp_y^{'}}{p_y^{'}} \tag{14}$$

where θ^* is a parameter defining how much the size of yield surface reduces during each unloading; p_y' is the loading variable that satisfies the following condition, i.e.,

$$p_y^{'} = p^{'} + \left(\frac{q}{M}\right)^2 \frac{1}{p^{'}} \tag{15}$$

Ni et al. (2015) extended this further and proposed θ^* as a function of number of cycles as follows:

$$\theta^* = \frac{1}{\xi_1 + N\xi_2} \tag{16}$$

where ξ_1 and ξ_2 are constants. While ξ_2 is shown to be dependent of loading frequency, the selection of ξ_1 has not been studied in great depth. Therefore, further work is needed to clarify how this parameter varies with soil type and loading properties.

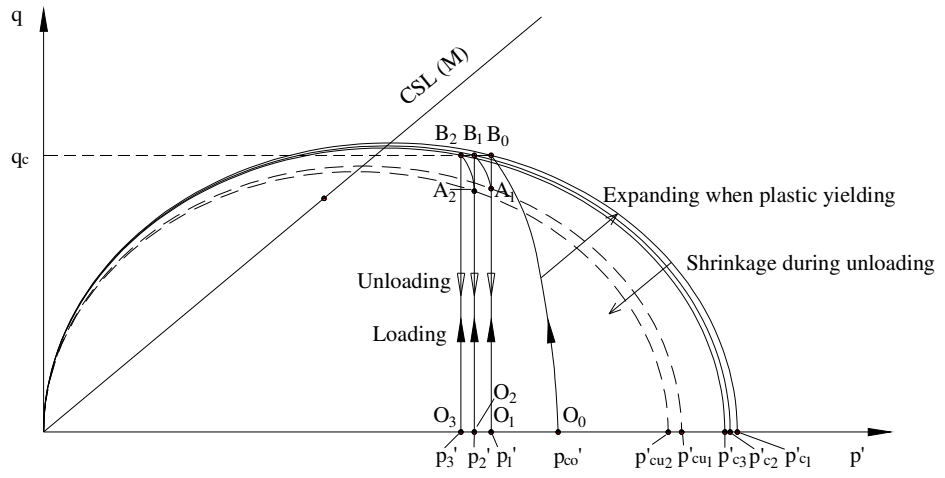

a)

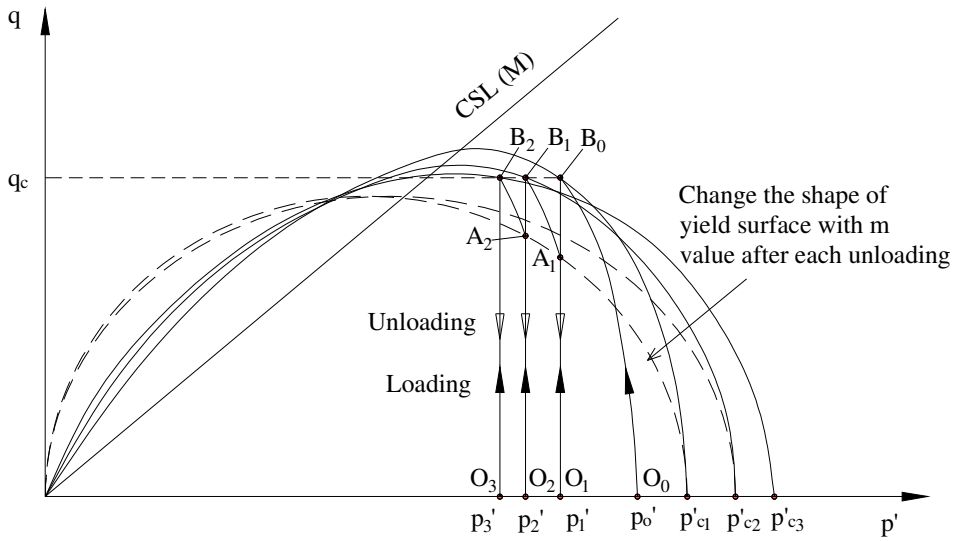

b)

Fig. 5 Response of yield surface to cyclic load: a) Model A, yield surface changes its size but remains elliptic shape; and b) Model B, yield surface changes its shape but remains its size

Fig. 5a demonstrates the variation in the stress path under cyclic loading based on Model A. In particular, the stress path moves from an initial stress point O_0 which is equivalent to an initial mean effective stress p'_o. In this demonstration, normally consolidated soil is assumed initially, so the yield surface expands to p'_{c1} as a

response to increasing q to q_c in the first cycle. The stress path reaches the given cyclic shear stress q_c (i.e., point B_0) then unloads to complete the first (one-way) cycle at O_1. During unloading, the yield surface shrinks to a new position, i.e., p'_{cu1} based on Eq. (14). In the next cycle, the stress path moves from O_1 to B_1, noting that the plastic strain begins to yield when the stress path hits the previous yield surface at A_1, resulting in a further expansion of the yield surface, i.e., with a size defined by p'_{c2}. Again, the yield surface expands its size to the new position before it shrinks back during subsequent unloading (i.e., p'_{cu2}). This process continues to occur with increasing number of cycles, resulting in reduced mean effective stress associated with increasing excess pore water pressure.

Model B: The shape of yield surface changes during cyclic loading

In this approach, the governing equation of yield surface is modified so that its shape is not purely elliptic. Specifically, the yield surface is governed by (McDowell and Hau 2004):

$$q^2 = \frac{M^2}{1-m} p'^2 \left[1 - \left(\frac{p'}{p'_{c0}} \right)^{2\left(\frac{1-m}{m}\right)} \right] \tag{17}$$

where *m* is the parameter which defines the shape of yield surface. Specifically, if *m* = 2, the yield surface is identical to the conventional MCC (i.e., elliptic shape, Eq. (10)); if *m* < 2 the shape of the yield surface slants to the right-hand side whereas it slants to the left if *m* > 2. It is assumed that under cyclic loading, *m* varies continuously with increasing number of load cycles (*N*), leading to an evolution in the shape of the yield surface. However, it is also assumed its size, i.e., p'_c, remains constant during unloading. As power functions are commonly used to empirically estimate the variation of soil properties such as soil stiffness with *N* in previous

studies (Matasovic and Vucetic 1992; Hyodo et al. 1994; Konstadinou and Georgiannou 2014; Ni et al. 2015), this approach is also adopted to establish the relationship between *m* and *N*. Specifically, the relationship between *m* and *N* is then proposed in this study as follows:

$$m = \frac{\alpha N^{0.5}}{N^{0.5} + \beta} \tag{18}$$

where α and β are the constants which depend on the nature of the cyclic loading and the properties of the soil. Apparently, *m* generally increases with increasing *N*, but it approaches the value α when *N* increases to a very large value, such as 50,000 cycles.

In this current study, the plastic potential is assumed to be identical to the yield surface, so the plastic potential is governed by (McDowell and Hau 2004):

$$\frac{d\varepsilon_p^p}{d\varepsilon_q^p} = \frac{M^2 - \eta^2}{m\eta} \tag{19}$$

Obviously, with $m = 2$, Eq. (18) returns to the conventional MCC model.

In this approach, the hardening rule of MCC model, i.e., Eq (12), is still valid. Because of the undrained condition ($d\varepsilon_p^e = -d\varepsilon_p^p$), Eq. (12) can be rewritten as

$$\kappa \frac{dp'}{p'} = -(\lambda - \kappa)\frac{dp_0'}{p_0'} \tag{20}$$

Furthermore, from Eq. (16), the following relationship can be obtained:

$$\frac{dp_0'}{p_0'} = \frac{dp'}{p'} + \frac{m\eta d\eta}{(m-1)\eta^2 + M^2} \tag{21}$$

Replacing Eq. (20) to Eq. (19), the rule governing the expansion of the generalized yield surface is then described by:

$$\frac{p_j^{'}}{p_{j+1}^{'}}=\left[\frac{(m-1)\eta_{j+1}^2+M^2}{(m-1)\eta_j^2+M^2}\right]^{\frac{m}{2(m-1)}\cdot\frac{\lambda-\kappa}{\lambda}} \tag{22}$$

where the subscripts *j* and (*j*+1) denote two consecutive loading stages involving increasing stress ratio.

Fig. 5b shows how the stress path evolves with increasing *N* with respect to the Model B. The yield surface expands to a new size, i.e., p'_{c1} at the first loading cycle following Eqs. (16) and (18). During unloading (from B_0 to O_1), the yield surface changes it shape while maintaining its size, i.e., p'_{c1}, which is different from Model A described above. In the next loading cycle, the yield surface reforms following the stress path $O_1A_1B_1$ to reach the desired level of q, resulting in a new shape and size of the yield surface (p'_{c2}). This process continues over increasing loading cycles, causing the plastic strain to increase which in turn causes an accumulation of EPWP. The peak of the yield surface moves gradually from the right towards the CSL as *N* increases. The major advantage of this Model is that the size of yield surface (p'_c) does not change during unloading (i.e., when the soil is fully elastic) while ensuring plastic yielding during loading, thus following the original concept of MCC model.

Fig. 6 shows the variation of *m* with the number of cycles *N* based on Eq. (17). It is apparent that *m* increases rapidly at the beginning then gradually slows down when *N* continues to increase. The ratio m/α approaches 1 when *N* increases toward infinity. Corresponding to the increase of *m* is the evolution in the shape of yield surface with increasing *N*. While the shape of yield surface slants from the right to the left when *N* increases, it is important to note that the yield surface changes its shape significantly during the initial stages when $m < 2$. Eq. (17) also indicates that increasing the parameter β results in smaller value of *m*, which means that the shape

of yield surface becomes distorted more in comparison to that of the conventional MCC (Fig. 6b).

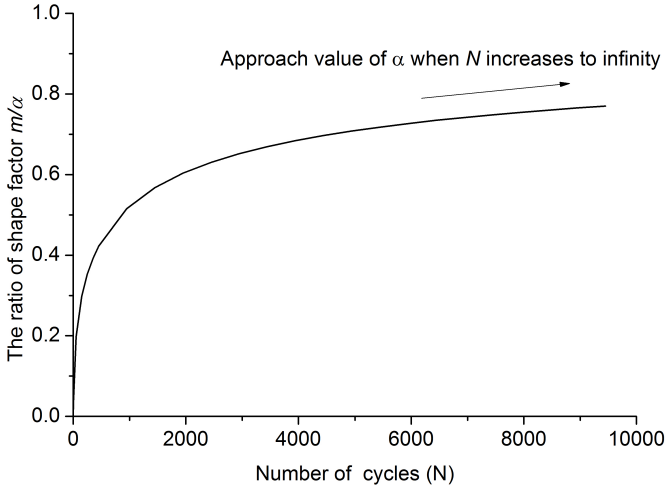

a)

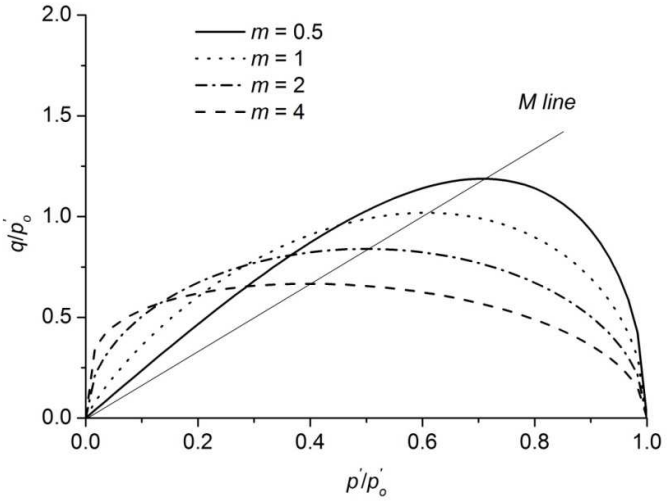

b)

Fig. 6 Evolution in the shape of yield surface with *m*: a) increasing *m* over *N*; b) change in the shape of yield surface with *m*

MODEL APPLICATIONS AND DISCUSSION

Model parameters

Experimental studies	Model parameters							Loading properties	
	λ	κ	M	ξ_1	ξ_2	α	β	CSR*	Frequency (Hz)
Series I (Ni et al. 2015)	0.18	0.03	1.68	2.7	280	10	435	0.1	1
				2.7	400	10	195	0.15	1
				2.8	550	10	135	0.2	1
				2.7	280	10	550	0.1	2
				2.7	400	10	250	0.15	2
				2.8	550	10	175	0.2	2
				2.7	280	10	700	0.1	5
				2.7	400	10	300	0.15	5
				2.8	550	10	240	0.2	5
Series II (Indraratna et al. 2020)	0.1	0.05	1.89	8	200	40	190	0.3	1
				8	800	40	575	0.5	1

***Note**: *The CSR defined by Ni et al. (2015) where CSR is the ratio between the applied cyclic stress and the initial shear strength of soil has been converted to the current CSR, i.e., Eq. (1).*

Table 2 Values of model parameters used in the predictions

Fundamental parameters used for MCC model such as M, λ and κ are determined from laboratory tests, i.e., static triaxial and consolidation tests. These values are shown in Table 1 for the clay soils considered in this study. Empirical parameters such as ξ_1, ξ_2, α and β governing the response of the yield surface are determined through a calibration process where the estimated EPWP and axial strain are compared with experimental results to ensure the highest accuracy over different sets of data. The values of these parameters are summarised in Table 2. How these

parameters change with loading and soil properties are discussed later in this paper, followed by empirical equations that may be adopted to estimate their values.

Predictions of EPWP and axial strain induced by cyclic loading

Fig. 7 compares the prediction made by the two models, i.e., Models A and B, with reference to experimental data (Ni et al. 2015) for f = 5Hz and CSR varying from 0.1 to 0.2 (Series I). The results indicate that the both models provide relatively good predictions while the predicted curve given by Model B appears to fit the experimental data slightly better, especially during the initial stages of cycling. For example, at 10,000 initial cycles, the accumulated normalised EPWP induced by a CSR of 0.2 is about 0.475 and 0.435, as estimated by Models A and B, respectively, which agrees well with the experimental data, i.e., a value of 0.46. The larger the CSR, the larger the accumulated EPWP, given the same number of loading cycles. At low number of cycles, especially when N < 6000 cycles, the results obtained by Model A, deviate significantly from the experimental values, whereas Model B provides more accurate predictions. For example, for N = 5000, while Model B agrees very well with experiment with an error less than 5%, Model A predictions indicate a difference of approximately 32%.

The two models can also capture well the inception of soil instability based on the development of axial strain under increasing number of cycles (N). Specifically, the experimental investigation (Ni et al. 2015) shows that for CSR = 0.2, the axial strain increases steeply when N reaches the critical level ($N_{c,i}$), i.e., approximately 30,000 cycles, which is represented well through the model outcomes. Indeed, both Models A and B estimate N_c at about 30,000 for CSR = 0.2, however, there is a distinct difference between the experimental and simulation data when N varies from

15,000 to 25,000 cycles. In stable specimens where CSR < CSR_c, there is a good agreement between the experimental results and model predictions.

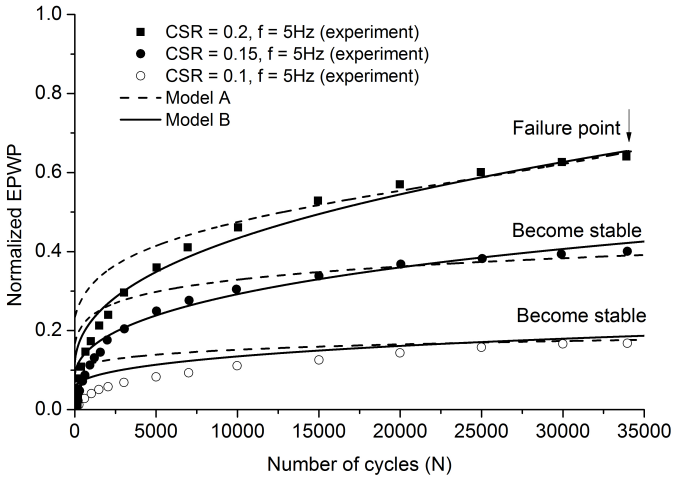

a)

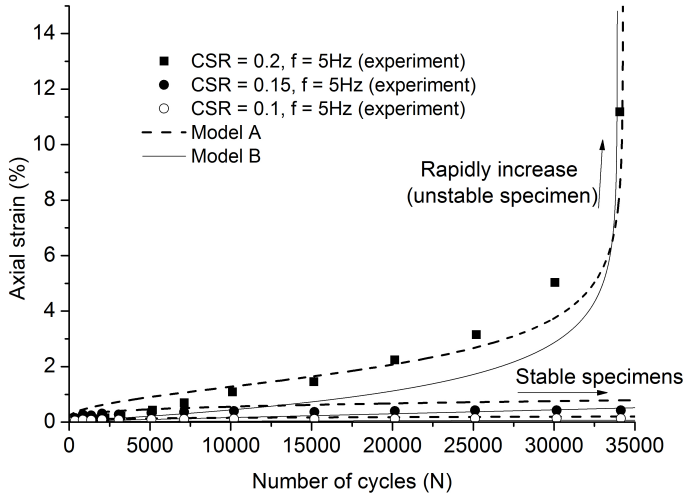

b)

Fig. 7 Comparison model outcomes using Models A and B: a) EPWP; and b) axial strain for the Kaolin clay soil (Series I) under a loading frequency f = 5 Hz, σ_c' = 25 kPa (Ni et al. 2015)

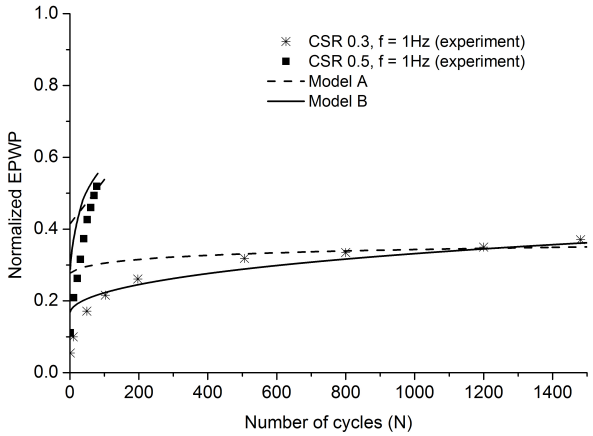

a)

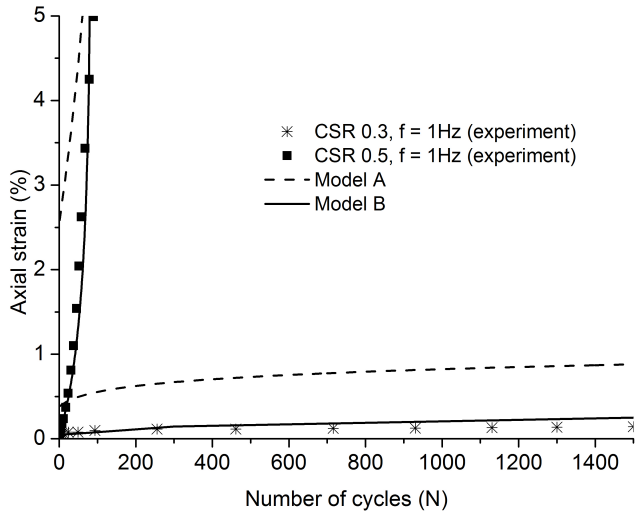

b)

Fig. 8 Comparison model outcomes using Models A and B: a) EPWP; and b) axial strain for the soil Series II, σ_c' = 15 kPa (Indraratna et al. 2020)

Fig. 8 shows the prediction of Models A and B for the experiment Series II on a silty soil (Indraratna et al. 2020b). For this low plasticity soil (i.e., PI = 11), Model B results in better predictions for both stable and unstable cases. Specifically, for stable specimens, i.e., CSR = 0.3, while the EPWP estimated by Model B is quite close to experimental data when *N* increases to 1500 cycles, values of EPWP predicted by Model A are significantly higher during the initial stage of cycling (*N* <

450). For unstable specimens, where EPWP increases steeply with increasing *N*, e.g., as CSR increases to 0.5, Model B also provides a more acceptable result. In response to this rapid development in EPWP, the axial strain increases rapidly to 5% during the first 100 cycles. There is a considerable difference in axial strain between the prediction of Model A and the experimental data, while Model B gives much better agreement at both levels of CSR, i.e., 0.3 and 0.5.

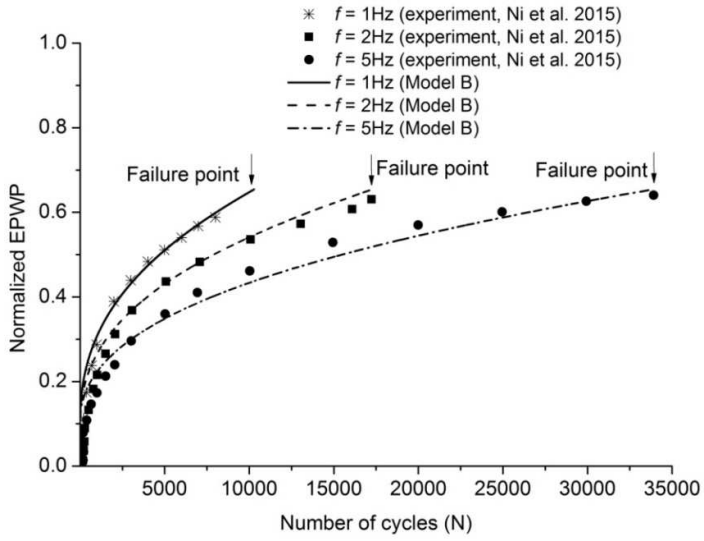

a)

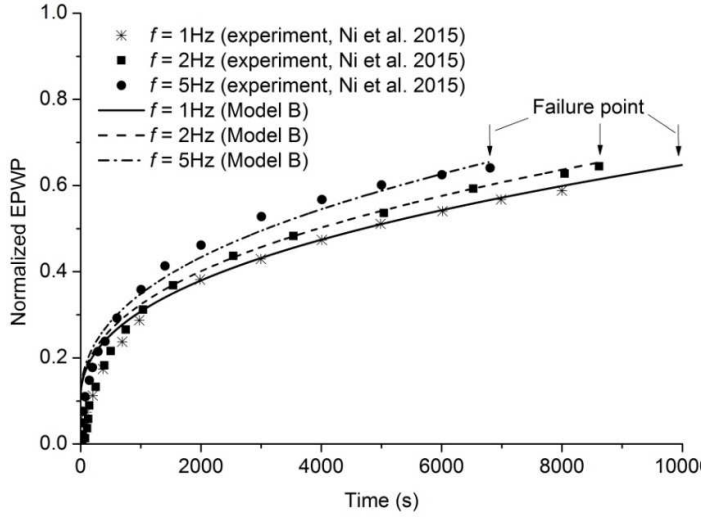

b)

Fig. 9 Influence of frequency on the accumulated EPWP - model and experimental results: a) EPWP over N; and b) EPWP over time (σ_c' = 25 kPa)

It is also noted that there is a distinct difference in cyclic behaviour in the two tested soils (Table 1) despite similar loading conditions. Specifically, for f = 1 Hz (see Fig. 9 for EPWP of the soil Series I) and at critical CSR_c, Kaolin clay soil (Series I with a PI of 22) requires about 7,500 cycles to trigger the instability, whereas the silty soil (Series II with a PI of 11) quickly becomes unstable (i.e., N just exceeds 30 cycles). This means that the lower the plasticity index, the earlier the soil becomes unstable at the critical value of CSR. This is logical, as soils with lower plasticity such as sandy to silty soils have little cohesive bonding between the soil particles, resulting in them being more vulnerable to increasing excess pore pressure (Nguyen and Indraratna 2020).

Influence of loading frequency and duration on accumulated EPWP

Fig. 9 represents how Model B can capture the influence of loading frequency on the accumulated EPWP. It is interesting that the smaller frequency causes EPWP to rise earlier considering the same number of loading cycles N. For example, f = 1Hz results in an EPWP of about 0.52, while f = 5Hz yields an EPWP of 0.35 after the same number of cycles, i.e., N = 5000. In addition, the soil reaches failure after a smaller number of cycles when the frequency decreases from 5 to 1 Hz. Specifically, the soil fails at N = 10,000, 16,000 and 34,000 when f increases from 1 to 2 and 5 Hz, respectively. This frequency-dependent behaviour agrees well with experimental data as shown in Fig. 4 and Fig. 9a.

It is also noted that when considering the development of EPWP with time, an opposite trend in which varying frequency affects the accumulated EPWP is shown in Fig. 9b. The loading with larger frequency results in a faster accumulation of EPWP. For example, the specimen tested at f = 5Hz develops a normalized EPWP

of 0.55 after 4000s, but the specimen tested at f = 1Hz takes about 6200s to achieve the same magnitude of EPWP. In other words, for a larger frequency loading, the specimen experiences an longer duration that the load (i.e., the average pressure induced by vertical load) acts on the specimen, making the EPWP reach a higher degree, thus earlier soil instability. The results indicate that a train of substantial axle load running at a higher speed (i.e., causing higher frequency cyclic loading) can lead to a faster and larger accumulated EPWP, thus triggering instability of the soil in shorter time. Note that despite this decisive role of loading duration in stimulating soil instability, in cyclic loading, it is more conventional to interpret deformation and pore water pressure results based on the frequency and the number of cycles (rather than the loading time) which are hence focused in the present study. Nevertheless, care should be taken properly when evaluating the effect of loading frequency and duration on cyclic response of soils.

Critical number of loading cycles

The critical number of cycles can normally be defined as the number of cycles required to cause soil to become either (*i*) unstable (i.e., the first type, $N_{c,i}$) or (*ii*) deformed to a predefined strain (i.e., the second type, $N_{c,s}$) (Georgiannou et al. 1991; Sakai et al. 2003; Indraratna et al. 2020a). In fact, for practical designs, the second approach is preferred where the largest allowable settlement and lateral deformation of soil structures are considered with respect to the safety and stability of overlying structures. For example, the critical number of cycles for subgrade under rail tracks can be considered with respect to a maximum vertical strain of about 1% rather than the attainment of an unstable state, i.e., failure of the soil.

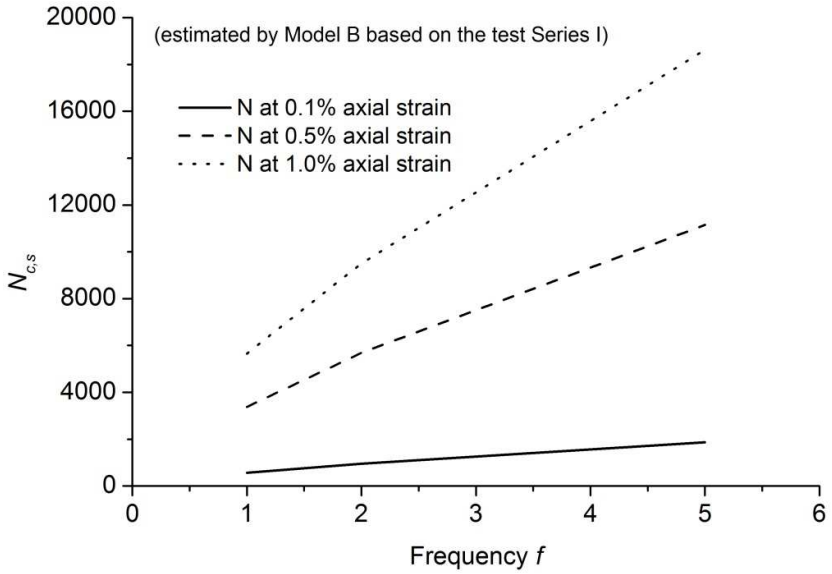

Fig. 10 Critical threshold of $N_{c,s}$ considering different levels of axial strain and frequency, captured by Model B based on the test Series I (i.e., PI = 22, σ_c'= 25 kPa, CSR = 0.2)

Previous sections have shown how the current proposed models can estimate the first type of critical number of cycles, i.e., $N_{c,i}$, with respect to different loading parameters (f and CSR, see Figs. 7, 8 and 9). This section discusses the variation of the second type, i.e., $N_{c,s}$, with different loading frequencies considering the accumulated axial (vertical) strain. Fig. 10 shows the estimated value of $N_{c,s}$ using Model B (based on the test Series I), considering axial strain levels of 0.1, 0.5 and 1%. The predicted results indicate that with increasing frequency, the value of $N_{c,s}$ also increases. However, the rate of increase in $N_{c,s}$ with increasing frequency, changes with different levels of critical strain. For example, for an axial strain of 0.1%, $N_{c,s}$ increases gradually with f but it increases more rapidly (i.e., the slope of the $N_{c,s}$ - f line becomes larger) when an axial strain of 1% is considered.

Characteristics of model parameters

Previous studies (Ni et al. 2015) have investigated characteristics of the parameters ξ_1 and ξ_2 used in Model A, so this section mainly focuses on the characteristics of parameters α and β which are adopted in the new Model B described in this paper. Ni et al. (2015) concluded that ξ_1 mainly depends on soil properties while ξ_2 varies with loading frequency (Fig. 11a). However, Ni et al. (2015) indicate insignificant influence of CSR on ξ_2, resulting in limited capacity of Model A in capturing the effects of different loading magnitudes on EPWP and axial strain, as shown in previous sections. Note that in this discussion, the predictions for the Kaolin soil (Series I) have been used to validate the model parameters, considering the significant quantity of experimental data available to identify the effects of the loading parameters *f* and *CSR*.

Fig. 11b presents the variation of parameter β used in Model B with the loading parameters, i.e., *f* and *CSR*. It is apparent that β changes significantly with different levels of *f* and *CSR*. Specifically, increasing CSR from 0.1 to 0.2 reduces the value of β from 435 to 135 for a loading frequency of 1Hz. The larger the loading frequency, the larger the value of β. For example, for a CSR of 0.1, β increases from 435 to 700. Based on these data, an empirical relationship between β and the loading parameters, i.e., *f* and CSR, is proposed as follows:

$$\beta = (36{,}000CSR^2 - 13{,}800CSR + 1455)f^{0.332} \quad (23)$$

Given specific values of *f* and CSR, Eq. (22) enables β to be computed so that Model B can be used to estimate how a soft soil responds to cyclic loading.

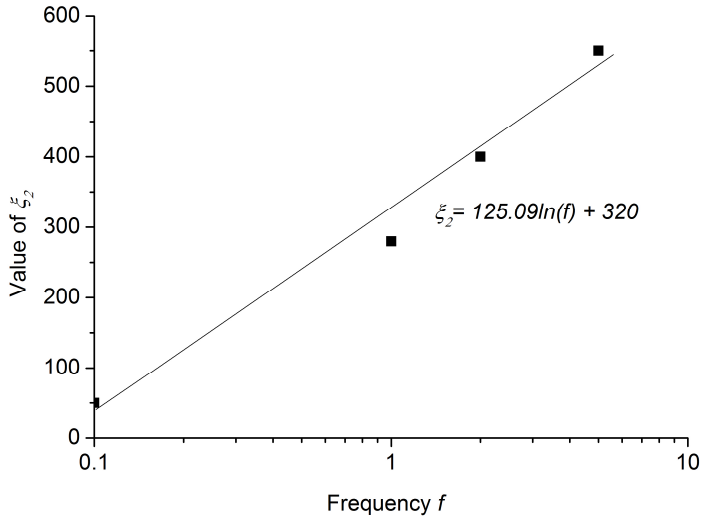

a)

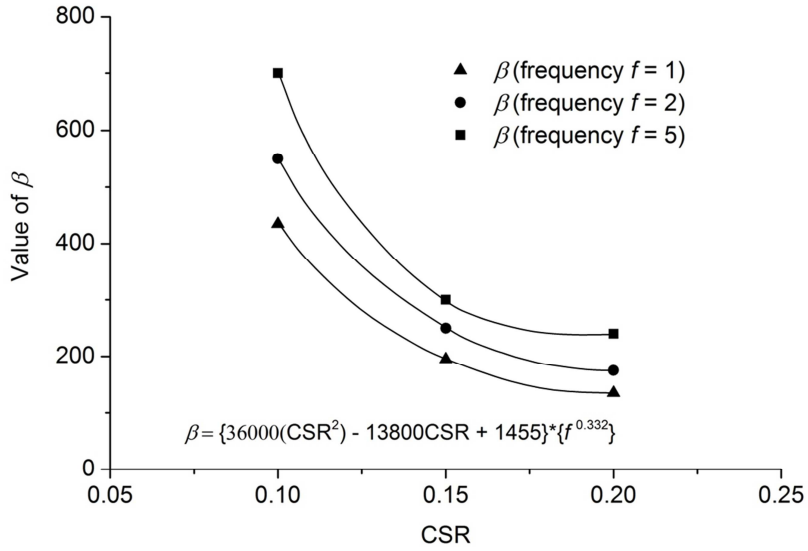

b)

Fig. 11 Variation of model parameters with loading parameters: a) ξ_2 of Model A with frequency (Ni et al. 2015), and b) β of Model B with frequency and CSR (based on the prediction outcomes for Kaolin soil Series I)

It is also noted that parameters ξ_1 and α in Models A and B mainly depend on soil properties. Table 2 shows that these parameters are unchanged when the same

soil is used during cyclic tests, but they seem to increase when the soil has lower plasticity. For example, ξ_1 increases from 2.8 to 8 and α increases from 10 to 40 when the PI of the soil decreases from 22 (Series I) to 11 (Series II). In previous sections, it was shown that EPWP tends to increase rapidly and reach an unstable stage quicker (i.e., at smaller $N_{c,i}$) for a soil having lower plasticity, which is why these model parameters are dependent on the soil properties in order to capture varying changes in the yield surface as N increases as represented by Eqs. (15) and (17). A recent study (Truong et al. 2021) where Model B is applied on different sets of experimental data (i.e., different type of soil and loading conditions) indicates that parameters α can be well determined based on empirical equations involving PI, the critical stress ratio M and initial stress state of the soil. Nevertheless, more effort is still needed to further validate these equations with a wider range of data so that they can be used with higher confidence for practical purposes.

The current study discusses two relatively simple approaches, i.e., Models A and B based on the conventional MCC model concepts which are widely used in practical designs nowadays. These models require only two additional parameters which can be determined based on empirical equations derived from soil and loading parameters. Model B which is an advanced version compared to the earlier Model A can be used to estimate the deformation (e.g., vertical deflection) of saturated subgrade soils under rail loads based on given soil and load properties. Furthermore, the model can predict the critical threshold of rail loads, i.e., the largest CSR (induced by the axle load) and number of cycles where soil becomes unstable with rapid increase in EPWP and axial strain, which is very essential for railway designs.

CONCLUSION

The current paper presented a discussion on the experimental and theoretical aspects of the cyclic response of subgrade soil under heavy haul-trains. Cyclic triaxial tests were used to examine two different soils, i.e., high plastic Kaolin clay (CH) and low plastic silty clay (CL) considering in situ rail loading conditions. Two different theoretical approaches, i.e., Models A and B, both based on the conventional Cam-Clay concepts, were proposed and discussed with their validation conducted using experimental data. The following conclusions can be drawn from this study:

- Increasing axle load (CSR) to a certain threshold (i.e., critical CSR_c) caused soil to reach an unstable stage where the excess pore water pressure (EPWP) and axial strain increase rapidly. For CSR < CSR_c, EPWP and axial strain maintained at a low constant level despite increasing number of cycles (i.e., cyclic stabilisation). For unstable specimens, i.e., CSR > CSR_c, soil with lower plasticity tended to reach instability quicker as opposed to soils with higher plasticity. The normalised EPWP was found to be around 0.6 to trigger the instability of soils.
- Loading frequency (*f*) has a significant effect on the cyclic behaviour of soils. The higher the loading frequency, the greater the number of cycles needed to trigger the instability of soil. However, increasing loading frequency (i.e., higher speed trains) is associated with a shorter time to cause soil instability when CSR > CSR_c.
- The two proposed Models A and B based on evolution in the size and shape of yield surface, respectively, showed considerable success in estimating EPWP and the development of axial strains in clay soil subjected to cyclic loads. The effects of loading and soil characteristics on the cyclic response of soil can be

captured relatively well, especially with Model B. However, there are limitations when using these models, especially Model A when used to predict the cyclic response of low plasticity soils.

- Model B showed more flexible and accurate predictions as its parameters better incorporated the effects of both loading frequency and CSR. An empirical equation was proposed to estimate the model parameter β based on given loading frequency and CSR for saturated clay soils. The lower the plasticity of soils, the larger the value of the parameter α.

CRediT Author Statements

Buddhima Indraratna: Writing-Review & Editing, Funding Acquisition, Resources; Conceptualization; **Thanh Trung Nguyen**: Conceptualization, Writing-Original Draft, Methodology, Formal analysis, Resources; **Mandeep Singh**: Writing-Original Draft, Writing-Review, Editing and Analysis; **Cholachat Rujikiatkamjorn**: Writing-Review, Editing and Analysis; **John P Carter**: Writing-Review, Editing and Analysis; **Ni Jing**: Conceptualization, Resources; **Minh Hoang Truong**: Conceptualization, Resources

Acknowledgements

This research was supported by the Australian Government through the Australian Research Council's Linkage Projects funding scheme (LP160101254), and the Transport Research Centre (TRC), University of Technology Sydney (UTS). The financial and technical support from SMEC, Coffey, ACRI, Sydney Trains and ARTC (Australian Rail Track Corporation) is much appreciated.

REFERENCES

ASTM D5311-92. 2004. Standard test method for load controlled cyclic triaxial strength of soil. American Society for Testing and Materials (ASTM), West Conshohocken, PA, Pa.

Baki, M.A.L., Rahman, M.M., Lo, S.R. and Gnanendran, C.T. 2012. Linkage between static and cyclic liquefaction of loose sand with a range of fines contents. Canadian Geotechnical Journal, **49**(8): 891-906. doi: 10.1139/t2012-045.

Carter, J., Booker, J. & Wroth. 1982. A critical state soil model for cyclic loading. *In* Soil mechanics-Transient and cyclic loads. *Edited by* G. N. Pande & Zienkiewicz, O. C. John Wiley & Sons Ltd, Chichester.

Chawla, S. and Shahu, J.T. 2016. Reinforcement and mud-pumping benefits of geosynthetics in railway tracks: Model tests. Geotextiles and Geomembranes, **44**(3): 366-380. doi: https://doi.org/10.1016/j.geotexmem.2016.01.005.

Duong, T.V., Cui, Y.-J., Tang, A.M., Dupla, J.-C., Canou, J., Calon, N. and Robinet, A. 2014. Investigating the mud pumping and interlayer creation phenomena in railway sub-structure. Engineering Geology, **171**: 45-58. doi: https://doi.org/10.1016/j.enggeo.2013.12.016.

Gens, A. and Potts, D.M. 1988. Critical state models in computational geomechanics. Engineering Computations, **5**(3): 178-197. doi: 10.1108/eb023736.

Georgiannou, V.N., Hight, D.W. and Burland, J.B. 1991. Behaviour of clayey sands under undrained cyclic triaxial loading. Géotechnique, **41**(3): 383-393. doi: 10.1680/geot.1991.41.3.383.

Hong, P.Y., Pereira, J.M., Cui, Y.J., Tang, A.M., Collin, F. and Li, X.L. 2014. An elastoplastic model with combined isotropic–kinematic hardening to predict the cyclic behavior of stiff clays. Computers and Geotechnics, **62**: 193-202. doi: https://doi.org/10.1016/j.compgeo.2014.07.008.

Hyodo, M., Yamamoto, Y. and Sugiyama, M. 1994. Undrained cyclic shear behaviour of normally consolidated clay subjected to initial static shear stresss. Soils and Foundations, **34**(4): 1-11. doi: 10.3208/sandf1972.34.4_1.

Indraratna, B., Korkitsuntornsan, W. and Nguyen, T.T. 2020a. Influence of Kaolin content on the cyclic loading response of railway subgrade. Transportation Geotechnics, **22**: 100319. doi: https://doi.org/10.1016/j.trgeo.2020.100319.

Indraratna, B., Nimbalkar, S., Christie, D., Rujikiatkamjorn, C. and Vinod, J. 2010. Field Assessment of the Performance of a Ballasted Rail Track with and without Geosynthetics. Journal of Geotechnical and Geoenvironmental Engineering, **136**(7): 907-917. doi: doi:10.1061/(ASCE)GT.1943-5606.0000312.

Indraratna, B., Rujikiatkamjorn, C. and Salim, W. 2011. Advanced Rail Geotechnology - Ballasted Track. CRC Press, The Netherlands. p.429.

Indraratna, B., Singh, M., Nguyen, T.T., Leroueil, S., Abeywickrama, A., Kelly, R. and Neville, T. 2020b. Laboratory study on subgrade fluidization under undrained cyclic triaxial loading. Canadian Geotechnical Journal, **57**(11): 1767-1779. doi: 10.1139/cgj-2019-0350.

Jefferies, M. and Been, K. 2015. Soil liquefaction: a critical state approach2nd ed. CRC Press. p.625.

Konstadinou, M. and Georgiannou, V.N. 2014. Prediction of pore water pressure generation leading to liquefaction under torsional cyclic loading. Soils and

Foundations, **54**(5): 993-1005. doi: https://doi.org/10.1016/j.sandf.2014.09.010.
Li, D. and Selig, E.T. 1996. Cumulative Plastic Deformation for Fine-Grained Subgrade Soils. Journal of Geotechnical Engineering, **122**(12): 1006-1013. doi: doi:10.1061/(ASCE)0733-9410(1996)122:12(1006).
Li, H.-e., He, Y.-j., Fan, G.-y., Li, T.-c. and Pastor, M. 2011. Recent developments of generalized plasticity models for saturated and unsaturated soils. Water Science and Engineering, **4**(3): 329-344. doi: https://doi.org/10.3882/j.issn.1674-2370.2011.03.009.
Li, T. and Meissner, H. 2002. Two-Surface Plasticity Model for Cyclic Undrained Behavior of Clays. Journal of Geotechnical and Geoenvironmental Engineering, **128**(7): 613-626. doi: doi:10.1061/(ASCE)1090-0241(2002)128:7(613).
Liu, J. and Xiao, J. 2010. Experimental Study on the Stability of Railroad Silt Subgrade with Increasing Train Speed. Journal of Geotechnical and Geoenvironmental Engineering, **136**(6): 833-841. doi: doi:10.1061/(ASCE)GT.1943-5606.0000282.
Mamou, A., Powrie, W., Priest, J.A. and Clayton, C. 2017. The effects of drainage on the behaviour of railway track foundation materials during cyclic loading. Géotechnique, **67**(10): 845-854. doi: 10.1680/jgeot.15.P.278.
Matasovic, N. and Vucetic, M. 1992. A Pore Pressure Model for Cyclic Straining of Clay. Soils and Foundations, **32**(3): 156-173. doi: https://doi.org/10.3208/sandf1972.32.3_156.
McDowell, G.R. and Hau, K.W. 2004. A generalised Modified Cam clay model for clay and sand incorporating kinematic hardening and bounding surface plasticity. Granular Matter, **6**(1): 11-16. doi: 10.1007/s10035-003-0152-8.
Mróz, Z., Norris, V.A. and Zienkiewicz, O.C. 1981. An anisotropic, critical state model for soils subject to cyclic loading. Géotechnique, **31**(4): 451-469. doi: 10.1680/geot.1981.31.4.451.
Nguyen, T.T. and Indraratna, B. 2019. Micro-CT scanning to examine soil clogging behavior of natural fiber drains. Journal of Geotechnical and Geoenvironmental Engineering, **145**(9): 04019037. doi: 10.1061/(ASCE)GT.1943-5606.0002065.
Nguyen, T.T. and Indraratna, B. 2020. The energy transformation of internal erosion based on fluid-particle coupling. Computers and Geotechnics, **121**: 103475. doi: https://doi.org/10.1016/j.compgeo.2020.103475.
Nguyen, T.T. and Indraratna, B. 2021. Rail track degradation under mud pumping evaluated through site and laboratory investigations. International Journal of Rail Transportation: 1-28. doi: https://doi.org/10.1080/23248378.2021.1878947.
Nguyen, T.T., Indraratna, B., Kelly, R., Phan, N.M. and Haryono, F. 2019. Mud pumping under railtracks: Mechanisms, Assessments and Solutions. Australian Geomechanics Journal, **54**(4): 59-80.
Nguyen, T.T., Indraratna, B. and Singh, M. 2021. Dynamic parameters of subgrade soils prone to mud pumping considering the influence of kaolin content and the cyclic stress ratio. Transportation Geotechnics, **29**: 100581. doi: https://doi.org/10.1016/j.trgeo.2021.100581.
Ni, J., Indraratna, B., Geng, X.-Y., Carter, J.P. and Chen, Y.-L. 2015. Model of Soft Soils under Cyclic Loading. International Journal of Geomechanics, **15**(4): 04014067. doi: doi:10.1061/(ASCE)GM.1943-5622.0000411.

Ouyang, Z. and Mayne, P.W. 2018. Effective friction angle of clays and silts from piezocone penetration tests. Canadian Geotechnical Journal, **55**(9): 1230-1247. doi: 10.1139/cgj-2017-0451.

Pastor, M., Zienkiewicz, O.C. and Chan, A.H.C. 1990. Generalized plasticity and the modelling of soil behaviour. International Journal for Numerical and Analytical Methods in Geomechanics, **14**(3): 151-190. doi: https://doi.org/10.1002/nag.1610140302.

Powrie, W., Yang, L.A. and Clayton, C.R.I. 2007. Stress changes in the ground below ballasted railway track during train passage. Proceedings of the Institution of Mechanical Engineers, Part F: Journal of Rail and Rapid Transit, **221**(2): 247-262. doi: 10.1243/0954409jrrt95.

Priest, J.A., Powrie, W., Yang, L., Grabe, P.J. and Clayton, C.R.I. 2010. Measurements of transient ground movements below a ballasted railway line. Géotechnique, **60**(9): 667-677. doi: 10.1680/geot.7.00172.

Roscoe, K.H. and Burland, J.B. 1968. On the generalized stress–strain behaviour of 'wet' clay.Engineering plasticity. Cambridge University Press, UK, 535–609.

Sakai, A., Samang, L. and Miura, N. 2003. Partially-drained cyclic behaviour and its application to the settlement of a low embankment road on sitly-clay. Soils and Foundations, **43**(1): 33-46. doi: 10.3208/sandf.43.33.

Sydney Trains. 2019. Annual report 2018-2019.

Tachibana, S., Ito, S. and Iizuka, A. 2020. Constitutive model with a concept of plastic rebound for expansive soils. Soils and Foundations, **60**(1): 179-197. doi: https://doi.org/10.1016/j.sandf.2020.02.007.

Trinh, V.N., Tang, A.M., Cui, Y.-J., Dupla, J.-C., Canou, J., Calon, N., Lambert, L., Robinet, A. and Schoen, O. 2012. Mechanical characterisation of the fouled ballast in ancient railway track substructure by large-scale triaxial tests. Soils and Foundations, **52**(3): 511-523. doi: https://doi.org/10.1016/j.sandf.2012.05.009.

Truong, M.H., Indraratna, B., Nguyen, T.T., Carter, J. and Rujikiatkamjorn, C. 2021. Analysis of undrained cyclic response of saturated soils. Computers and Geotechnics, **134**: 104095. doi: https://doi.org/10.1016/j.compgeo.2021.104095.

Wood, D.M. 1990. Soil behaviour and critical state soil mechanics. Cambridge University Press,

Zhao, H.Y., Indraratna, B. and Ngo, T. 2021. Numerical simulation of the effect of moving loads on saturated subgrade soil. Computers and Geotechnics, **131**: 103930. doi: https://doi.org/10.1016/j.compgeo.2020.103930.

Zienkiewicz, O. and Mróz, Z. 1984. Generalized plasticity formulation and applications to geomechanics. *In* Mechanics of engineering materials. *Edited by* Desai CS and Gallagher RH. Wiley, New York. pp. 655–679.